ACS Catalysis

Research Article

pubs.acs.org/acscatalysis

Electrodeposited Zn Dendrites with Enhanced CO Selectivity for Electrocatalytic CO_2 Reduction

Jonathan Rosen, Gregory S. Hutchings, Qi Lu, Robert V. Forest, Alex Moore, and Feng Jiao*

Center for Catalytic Science & Technology (CCST), Department of Chemical and Biomolecular Engineering, University of Delaware, Newark, Delaware 19716, United States

Supporting Information

ABSTRACT: Electrochemical CO_2 reduction is a key reaction for CO_2 conversion to valuable fuels and chemicals. Because of the high stability of the CO_2 molecule, a catalyst is typically required to minimize the energy input and improve reaction rates needed for device level commercialization. In this paper, we report a nanostructured Zn dendrite catalyst that is able to electrochemically reduce CO_2 to CO in an aqueous bicarbonate electrolyte with greatly enhanced properties. The catalytic activity is over an order of magnitude higher than that of bulk Zn counterparts, with a CO faradaic efficiency around 3-fold higher. The stability of the Zn electrode under realistic CO_2 electrolysis conditions was explored using scanning electron microscopy and in situ/operando X-ray absorption spectroscopy techniques. The results clearly demonstrate that nanostructured and bulk Zn catalysts are structurally stable at potentials more negative than −0.7 V versus RHE, whereas severe chemical oxidation occurs at more positive potentials.

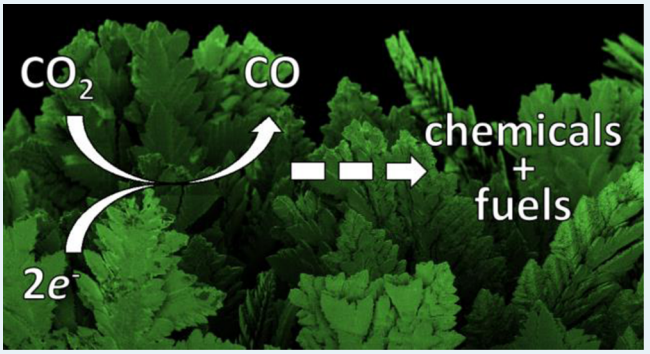

KEYWORDS: *electrocatalysis, CO_2 reduction, Zn, electrodeposition, X-ray absorption spectroscopy*

INTRODUCTION

CO_2 conversion through electrochemical approaches has been suggested as a promising method of creating high-value products from highly unwanted CO_2 sources. Because CO_2 is a thermodynamically stable molecule, a suitable catalyst could significantly reduce the energy penalty that is required to activate it.[1−3] To date, researchers have identified several bulk metallic catalysts, such as Cu, Ag, Au, and Zn, which are able to reduce CO_2 electrochemically to more reactive molecules in aqueous electrolytes.[4−7] Among all the bulk metallic catalysts, Au, Ag, and Zn are known to be selective for CO_2 to CO conversion, though large overpotentials are required to obtain a decent CO current (i.e., reaction rate).[4,8] In the past few years, nanostructured catalysts have attracted much attention for CO_2 to CO conversion due to their high catalytic surface area and unique properties compared to their polycrystalline counterparts.[9−15] We recently reported a nanoporous silver catalyst, which is able to electrochemically convert CO_2 into CO in a very selective and efficient way.[16] The nanoporous structure creates an extremely large surface area for catalytic reaction, and the curved internal surface generates a large number of highly active step sites for CO_2 conversion, resulting in an exceptional activity that is over 3000 times higher than that of the polycrystalline counterpart at a moderate overpotential. However, Ag is an expensive element and not ideal for commercial applications at large scale (terawatt), and therefore, it is crucial to identify catalysts based on non-precious elements with high CO selectivity.

Zn is an earth-abundant metal and is more than 2 orders of magnitude cheaper than Ag. Early work by Hori and Ikeda have shown some promising properties of bulk metallic Zn as an active electrocatalyst for CO_2 reduction to primarily CO.[17−19] At a potential of −1.14 V versus the reversible hydrogen electrode (RHE), a CO current density of ∼4 mA cm^{-2} was reported by both Hori and Ikeda. However, the reported CO faradaic efficiencies (i.e., CO selectivities) for Zn catalysts vary over a wide range, from 40% to 80%.[5,18] Although effects such as contamination of the electrolyte and the purity of Zn electrode could affect selectivity, the inconsistencies in previous studies were more likely caused by the oxidation and dissolution of the surface of the Zn electrode under testing conditions. Zn can be easily oxidized in contact with air, moisture, and through prolonged contact with aqueous electrolytes, having a significant effect on catalytic activity. Past work by Ikeda manipulated this phenomena and showed increased CO production rates achieved through intentional dissolution of Zn prior to electrolysis and a likely redeposition process.[18] The source of the improved catalytic activity was not well explored but is likely a product of new electrodeposited Zn

Received: May 4, 2015
Revised: June 10, 2015
Published: June 19, 2015

DOI: 10.1021/acscatal.5b00922
ACS Catal. 2015, 5, 4586−4591

sites formed on the electrode surface. A dedicated and thorough experimental effort is required to explore the origin of the discrepancy in CO faradaic efficiencies in the literature.

Here, we report a nanostructured Zn dendrite electrocatalyst, which was synthesized using an electrodeposition method to minimize the surface oxide layer formation and to create a highly active catalyst with a dendritic structure. The resulting Zn dendrite required a potential of −0.9 V (vs RHE. unless noted all the voltages reported here are against RHE) to achieve a CO current density of 4 mA cm^{-2}, which is ∼250 mV less negative than that of bulk Zn catalyst. Remarkably, the CO faradaic efficiency of Zn dendrite catalyst (∼80%) is around three times higher than that of bulk Zn foil. Moreover, in situ/operando X-ray absorption spectroscopy (XAS) techniques were used for the first time in studying CO_2 electrolysis. The results confirmed that the Zn catalysts exhibited good stability at potentials more negative than −0.7 V, whereas at less negative potentials, they were readily oxidized under CO_2 electrolysis conditions, which is likely the origin of selectivity and stability issues associated with Zn catalysts.

EXPERIMENTAL SECTION

Electrode Preparation. Zn foil (Alfa Aesar, 99.994%, 0.25 mm) electrodes were prepared by mechanical polishing using sandpaper (400 grit), followed by sonication in acetone and water. The foils were then attached to a nickel wire using silver paint. Nanostructured Zn dendrite electrodes were prepared using a modified procedure for electrochemical Zn deposition. In a typical synthesis, ZnO powder (Sigma-Aldrich, 99.999%) was dissolved in 6 M KOH (Sigma-Aldrich, 99.99%) to form a precursor solution for Zn deposition.[20] Zn foil electrodes were then used as a substrate for electrochemical Zn deposition. A chronopotentiometry experiment set at −1.0 A/cm^2 for 60 s was used to reduce the Zn precursor to metallic Zn on the surface of the previously prepared Zn foil electrodes. Following deposition, the electrodes were rinsed in deionized water and immediately used for electrochemical testing to prevent oxidation of the Zn electrodes. Samples for structural characterizations were immediately transferred and characterized to minimize exposure to atmospheric air.

Structural Characterization. Powder X-ray diffraction (PXRD) measurements were performed using a PANalytical X'Pert X-ray diffractometer using Cu Kα radiation. Scanning electron microscopy (SEM) images were collected using a Zeiss Auriga-60. A Phi 5600 X-ray photoelectron spectroscopy (XPS) system was used to analyze the surface properties. The system is equipped with a multichannel hemispherical analyzer and Al anode X-ray source. The binding energy scale was calibrated by comparing the position of the primary photoelectron peaks in Cu, Au, and Ag reference foils to values in literature. Data was analyzed using CasaXPS software, and peaks were fit using a Gaussian/Lorentzian product line shape and Shirley background. Transmission electron microscopy (TEM) studies were performed with a JEOL JEM-2010F using an accelerating voltage of 200 kV. Surface areas of dendritic and bulk Zn electrodes were measured using krypton gas adsorption and atomic force microscopy (Dimension 3100, Veeco Instruments Inc.), respectively. The results (Figures S1 and S2) confirmed that Zn dendrite electrodes have a typical surface area of around 90 cm^2/cm^2_{Geo}, corresponding to over 80 times higher surface area than Zn bulk foil electrodes.

Electrochemical Testing. A Princeton Applied Research VersaSTAT 3 potentiostat was used for all electrochemical testing. CO_2 reduction experiments were performed in a gastight two-compartment electrochemical cell separated by a piece of anion exchange membrane (Fumasep, FAA-3). The bicarbonate electrolyte was prepared by purging an aqueous solution of sodium carbonate (Fluka, ≥99.9999) overnight with high purity CO_2 gas (Matheson, 99.999%). The final electrolyte was 0.5 M $NaHCO_3$ saturated with CO_2 (pH = 7.2). A platinum wire was used as the counter electrode and Ag/AgCl (3.0 M NaCl saturated with AgCl, BASi) as the reference electrode. The reference electrode potentials were converted to RHE using the formula E (RHE) = E (Ag/AgCl) + 0.210 V +.0591 V × pH. Prior to electrolysis, the bicarbonate electrolyte was purged with CO_2 gas for at least 30 min. The electrolyte in the cathodic compartment was stirred to help the diffusion of reactants and products. Quantification of gas-phase products was performed using a gas chromatograph (Shimadzu, GC-2014) equipped with a PLOT MolSieve 5A column and a Q-bond PLOT column. Helium (Keen Gas, 99.999%) was used as the carrier gas. Gas-phase products were collected every 30 min using a gastight syringe (Hamilton) to assess catalyst selectivity and total partial current density. Liquid product analysis was measured using a Bruker AVIII 600 MHz nuclear magnetic resonance (NMR) spectrometer. In a typical NMR analysis, a 500 μL electrolyte was sampled at the conclusion of the electrolysis and mixed with 100 μL D_2O, with 100 ppm (m/m) dimethyl sulfoxide (DMSO, Alfa Aesar, ≥99.9%) added as the internal standard. The 1D ^{1}H spectrum was measured with water suppression using a presaturation method.

Constant potential electrolysis was used to measure the activity of the Zn electrodes. For experiments at potentials more positive than −1.1 V, we added a 10 min pre-reduction process, in which the electrode was treated at −1.1 V to remove any native oxide layer formed on the surface. During this pre-reduction step, the headspace of the electrochemical cell was purged with CO_2 to remove any gas-phase products formed. After the pre-reduction step, the cell was sealed airtight and set at the desired potential for a 3 h electrolysis experiment. For the Tafel plot, the average current and CO efficiency acquired after 30 min of electrolysis was used for consistency.

In Situ/Operando XAS Experiments. X-ray absorption experiments were performed at beamline X18A at the National Synchrotron Light Source (NSLS) at Brookhaven National Laboratory (BNL) through the general user program. The XAS data was processed using the IFEFFIT package, including Athena and Artemis.[21] A modified two-compartment H-type electrochemical cell made from Teflon was used for in situ/operando XAS experiments and is shown in (Figure S3). A small window was cut out on the cathode side and sealed with Kapton film to allow fluorescence signals to pass from the electrode to the detector. For these XAS experiments, Zn dendrite electrodes were instead deposited on Ti foil (Alfa Aesar, 99.998%) to avoid signal from the bulk substrate.

RESULTS

Electrodeposition is known to be an effective method to synthesize metallic Zn materials with a variety of architectures.[20,22] We first investigated how the electrodeposition conditions affect the Zn electrode morphology by tuning the deposition rate relative to Zn ion diffusion to the electrode surface. At low deposition rates (∼10 mA cm^{-2}), where Zn ion diffusion to the surface is much faster than the rate of deposition, Zn filaments had a mossy morphology (Figure S4). The mossy structure is very fragile and cannot survive in the

DOI: 10.1021/acscatal.5b00922
ACS Catal. 2015, 5, 4586−4591

gas-evolving CO_2 electrolysis process. Increasing the deposition rate to an intermediate region (~20 mA cm^{-2}) resulted in bulky electrodes with low surface area (Figure S5). In contrast, when an extremely fast electrodeposition rate (~1.0 A cm^{-2}) was used, Zn dendrites with highly branched nanostructures can be formed (Figure 1a). Based on the cross-section scanning electron microscopy (SEM) image (Figure 1a), the dendrite layer was approximately 50−100 μm thick and uniformly coated on the Zn substrate. The formation of Zn dendrites is likely driven by the high deposition rate, which created a low Zn concentration environment near the electrode surface and forced the dendrite to grow outward toward high Zn concentration regions. The current−morphology relationship in Zn electrodeposition is consistent with reports from other groups.[20,22]

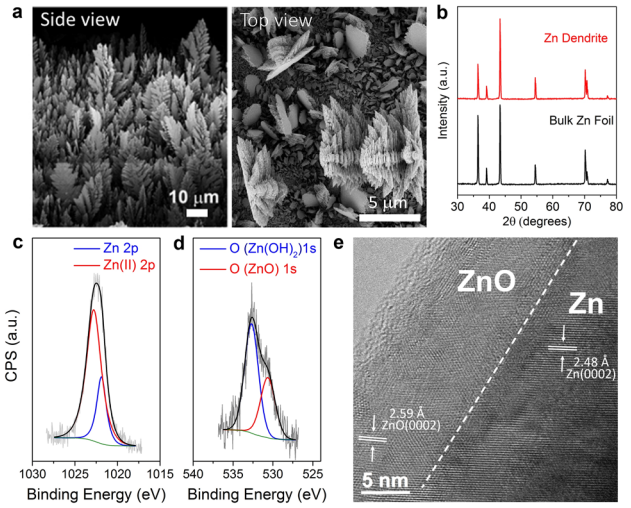

Figure 1. (a) Typical SEM image for a Zn dendrite catalyst. (b) PXRD patterns of bulk and dendritic Zn electrodes. (c) Zn 2p and (d) Zn 1s XPS results for as-made Zn dendrite catalyst. (e) A typical HRTEM image for a Zn dendrite catalyst.

The crystalline structure of the as-prepared Zn dendrite electrocatalyst was first examined using powder X-ray diffraction (PXRD). The PXRD diffraction pattern in Figure 1b clearly confirmed the highly crystalline nature of the as-prepared Zn dendrite catalyst. All the diffraction peaks are well-defined and aligned precisely with the pattern for Zn bulk foil (Figure 1b), indicating a phase-pure metallic Zn (JCPDS file#: 00−004−0831). We also characterized the surface of the Zn dendrite electrocatalyst using X-ray photoelectron spectroscopy (XPS), because the surface layer could significantly influence the electrocatalytic properties. The XPS results for as-prepared Zn dendrite catalyst at Zn 2p and O 1s regions are shown in Figure 1c,d. Although the PXRD data suggested that the sample is mainly metallic Zn, a significant amount of Zn^{2+} and O^{2-} were observed in the as-prepared sample, indicating that the surface is not truly metallic. It should be noted that Zn dendrite can be readily oxidized in the presence of air or moisture. Although we dried the as-prepared Zn samples under vacuum immediately after electrodeposition and kept them inside an argon protected glovebox, it is likely impossible to avoid exposing the electrode to water vapor during vacuum drying, which oxidized the Zn surface. Even after prolonged sputtering inside the XPS chamber, Zn^{2+} and O^{2-} can still be detected in as-prepared Zn catalyst (Table S1), indicating a thick layer of Zn oxide. Because of the water effect and the reducing environment of CO_2 electrolysis, the true surface of Zn dendrite under working conditions may not be the same as what we observed in ex situ XPS measurements (Table S1).

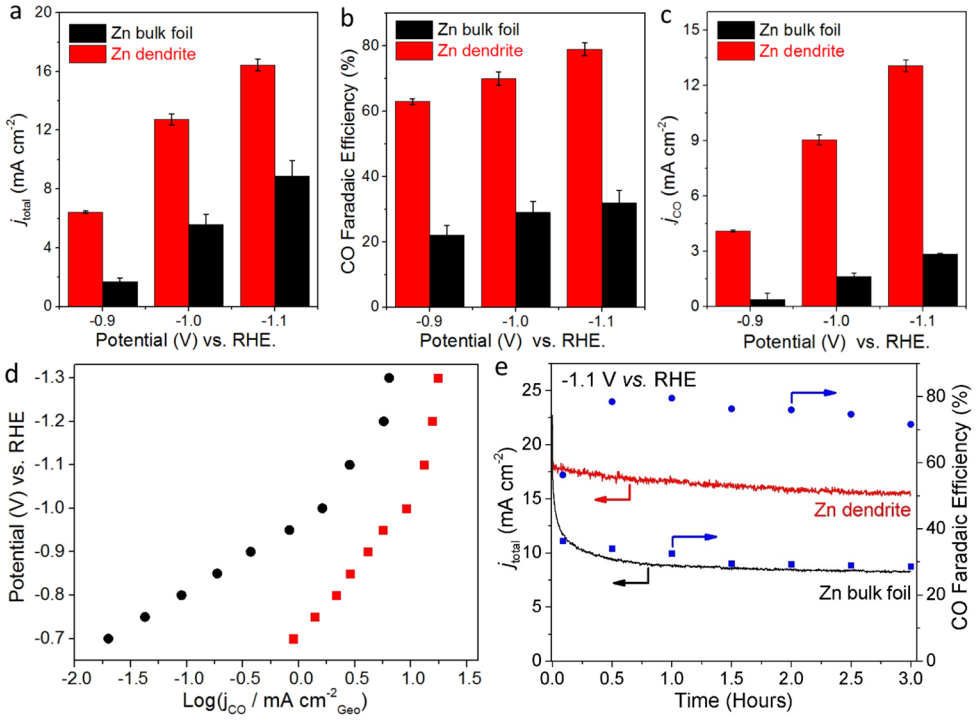

Figure 2. Comparison of (a) total current density, (b) CO faradaic efficiency, and (c) CO current density for bulk and dendritic Zn electrocatalysts. (d) Plot of log (j_{CO}) vs potential for Zn bulk foil (black) and Zn dendrite (red). (e) Constant potential studies of bulk and dendritic Zn catalysts at −1.1 V vs RHE. The bulk symbols represent the CO faradaic efficiencies.

DOI: 10.1021/acscatal.5b00922
ACS Catal. 2015, 5, 4586−4591

Therefore, we performed in situ and operando XAS experiments and the results will be discussed together with electrocatalytic CO_2 reduction data.

In order to gain additional insights into the catalytically active exposed surface of the Zn dendrites, HRTEM studies were conducted on as-prepared structures (Figure 1e). Near the surface of the dendrites, a thin (1−2 nm) amorphous layer can be observed, followed by a thicker polycrystalline layer (∼10 nm) with apparent *d*-spacings consistent with ZnO. Beneath this layer, highly crystalline metallic Zn can be observed, forming the core of the dendrite and the vast majority of the deposited mass. The *d*-spacings for Zn and ZnO (0002) facets are indicated on Figure 1e. Due to the ZnO layer, the surface of the dendrites should be polycrystalline Zn following conversion under the highly reducing conditions of electrochemical CO_2 reduction. Therefore, correlating the surface structure of the dendrites with activity on the basis of observed dendrite growth directions is difficult, as exposed facets under operating conditions are independent of the preferred orientation in the Zn core.

Electrochemical CO_2 reduction using Zn catalysts was carried out using constant potential electrolysis in a two-compartment H-type electrochemical cell separated by an anion exchange membrane. A 0.5 M sodium bicarbonate aqueous solution saturated with CO_2 (pH = 7.2) was used as the electrolyte. In addition, the headspace of the cathodic compartment was purged with CO_2 and sealed before the electrolysis. Partial current densities of CO_2 reduction products were calculated on the basis of GC and NMR analyses. The two primary products under testing conditions are CO from the reduction of CO_2 and H_2 as a byproduct from the concurrent proton reduction reaction. A very small amount of formate was also detected (see details in Table S2). Figure 2a shows that the Zn dendrite catalyst exhibited a total current density approximately two times as high as that of Zn bulk foil, which is due to the likely higher surface area that one would expect for a highly nanostructured electrocatalyst compared to a bulk foil. Additionally, a much higher CO selectivity almost 3 times higher was observed for Zn dendrite catalysts at moderate potentials (0.9−1.1 V) compared to that for bulk foil (Figure 2b). Combining the high total currents and excellent CO selectivity, the Zn dendrite electrode is able to deliver over an order of magnitude higher CO partial current density (4−14 mA cm^{-2}) compared to that of Zn foil electrode (0.3−2.8 mA cm^{-2}), which is evident in Figure 2c. A maximum CO faradaic efficiency at 79% has been achieved using a Zn dendrite electrode at a potential of −1.1 V. In sharp contrast, the bulk Zn foil exhibited a CO faradaic efficiency lower than 35%, consistent with values reported in previous publications.[19] On the basis of the H_2 partial current density results shown in Figure S6, it is clear that hydrogen evolution is suppressed by Zn dendrite catalyst. We speculate that the origin of hydrogen evolution suppression in nanostructured Zn dendrite catalyst is potentially due to a higher density of stepped sites compared to bulk Zn foil. The high density of stepped sites on the curved Zn dendrite surface is likely created through the electrodeposition of Zn ions. Suppression of hydrogen evolution by stepped surface has been observed in Pb and Cu catalysts for CO_2 reduction.[13,23] In addition, improved preparation of the catalyst followed by immediate transferring for testing may prevent degradation of the highly sensitive Zn surface, significantly improving catalytic activity.

To compare intrinsic activities of bulk Zn foil and Zn dendrite catalyst, we measured their surface areas so that we could estimate a CO production rate per active site. On the basis of the surface area measurements (see Experimental Section), we would expect a 90 times difference in CO production rates, whereas the observed differences in CO current densities are significantly less than the expected increase (∼45 times at −0.7 V, Figure 2d). One possibility is that the Zn dendrite surface may not be fully accessible by electrolyte and CO_2, especially because gas products are produced during electrolysis. Therefore, the surface area effect may be overestimated and more similar to the 45 times increase in CO current density observed. It is then likely that bulk and dendritic Zn have a similar turnover frequency per surface site, and the observed high CO current density for Zn dendrite catalyst is mainly due to its higher surface area. Because the electrodeposited Zn dendrite catalyst has not only a very high surface area, but also an enhanced CO selectivity, it is able to display activities which are more than 1 order of magnitude higher for CO_2 reduction to CO while suppressing the highly undesired hydrogen.

To gain kinetic insights for CO_2 reduction to CO on Zn catalysts, we measured CO current density at various overpotentials and constructed Tafel plots for both bulk and dendrite Zn electrodes (Figure 2d). The Tafel slopes are ∼155 and ∼260 mV/dec for bulk Zn foil and Zn dendrite, respectively. It is evident that the slopes for both Zn catalysts are significantly higher than those values reported for other electrocatalysts that selectively reduce CO_2 to CO under similar conditions.[24,25] It is known that surface coverage of intermediates and mass transport may strongly affect Tafel slope. In an ideal Tafel analysis, electrodes should be operated under relatively low currents (i.e., low overpotentials) to avoid any nonkinetic effect, such as mass transport of reactants and products both to and from the electrode surface. We attempted to measure CO partial current at lower overpotentials, but we observed an inherently unstable nature of the Zn electrodes at potentials less negative than −0.7 V. At those potentials, oxidative currents were observed for the Zn dendrite catalyst (Figure S7). We suspect that dissolution and/or chemical oxidation of the Zn electrodes may occur at significantly lower overpotentials, because the spontaneous reaction of metallic Zn with H_2O to form ZnO and H_2 becomes thermodynamically favorable. It should be noted that at −1.1 V the Zn electrodes exhibited stable currents and CO faradaic efficiencies over a period of 3 h CO_2 electrolysis (Figure 2e). Long-term stability study beyond 3 h will require a flow cell because accumulated CO product in headspace will alter CO_2 partial pressure and a notable portion of CO_2 will be consumed.

To further examine the stability of the Zn catalyst and identify a stable operating window, further structural characterizations have been performed on the Zn catalysts at various potentials. Typical SEM images for Zn dendrite catalyst after CO_2 electrolysis at −0.5, −0.7, −0.9, and −1.1 V are shown in Figure S8. It can be seen that at −0.5 V, large crystal-like particles with a size of 5−10 μm were formed (see blue arrows in Figure S8a). At the same time, small clusters with a size of ∼0.1 μm were also found on dendritic particles (pointed out by yellow arrows in Figure S8a). Although we cannot identify the structure or composition of the particles using SEM and energy dispersive spectroscopy technique, we believe that both large and small clusters are dissolved and redeposited Zn, zinc oxide, or zinc hydroxide. Note that only a few small clusters (yellow

DOI: 10.1021/acscatal.5b00922
ACS Catal. 2015, 5, 4586−4591

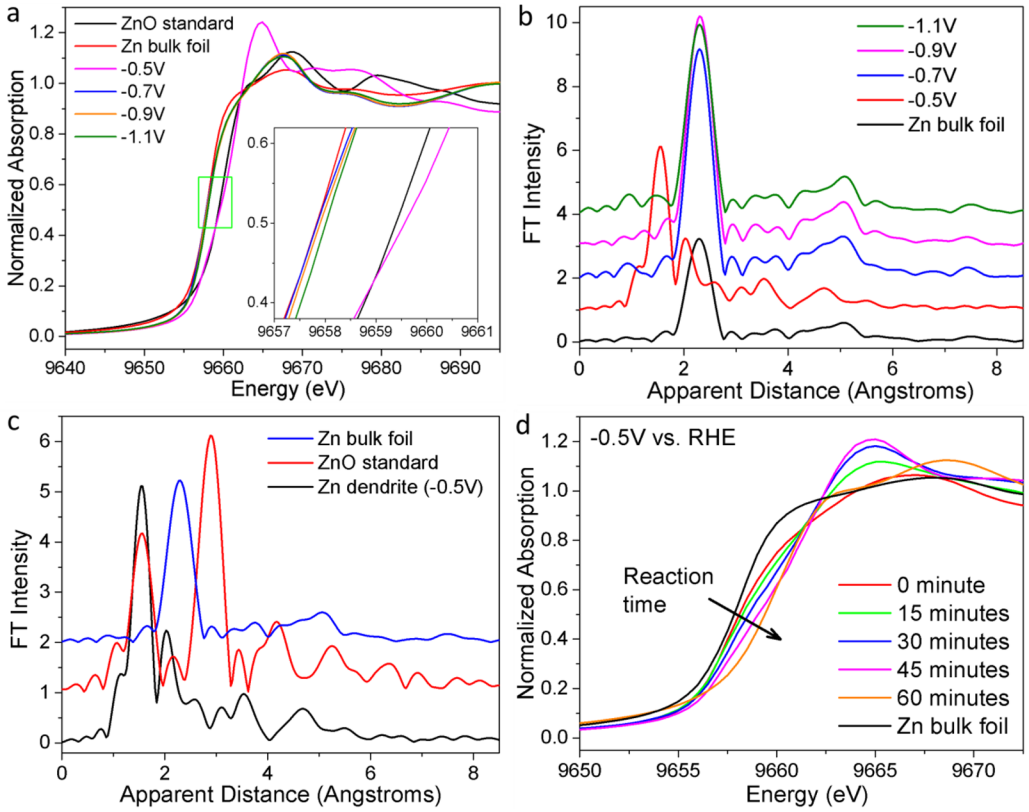

Figure 3. In situ (a) XANES and (b, c) EXAFS data for dendritic Zn electrodes operated at various potentials for 1 h. (d) In operando XANES data for Zn dendrite electrode at −0.5 V. Data for bulk Zn and ZnO are also included for comparison.

arrows in Figure S8b) can be observed for the catalyst after electrolysis at −0.7 V, and no obvious change was observed for catalysts reacted at −0.9 and −1.1 V, suggesting that the stability limit for Zn dendrite catalyst is approximately −0.7 V. The SEM results agree well with our CO_2 electrolysis data.

We also carried out in situ XAS experiments to investigate the stability of the Zn dendrite catalyst at various potentials using a customized electrochemical cell (Figure S3), which allowed us to collect XAS data under working conditions. We first held Zn dendrite electrode in the customized cell at a constant potential for 1 h. After the completion of CO_2 electrolysis, the Zn electrode was kept in the cell and XAS data was collected immediately and in situ. All the X-ray absorption near-edge spectroscopy (XANES) results collected at −0.5, −0.7, −0.9, and −1.1 V are shown in Figure 3a. Data for bulk Zn and ZnO are also shown for comparison. It is clear that the Zn K-edge of electrode operated at −0.5 V has a significant shift toward the binding energy for Zn^{2+}, suggesting that Zn dendrite was fully oxidized to Zn^{2+} within 1 h of electrolysis. In contrast, at a potentials more negative than −0.7 V, Zn dendrite electrodes remained Zn^0, and no obvious K-edge shift can be observed, indicating a likely stable operating window for the Zn dendrite catalyst. Turning to the extended X-ray absorption fine structure (EXAFS) data, a well-defined peak at ∼2.3 Å was observed for Zn dendrite electrodes operated at −0.7, −0.9, and −1.1 V (Figure 3b). The Zn electrode at −0.5 V, however, had two distinct peaks at 1.55 and 2.03 Å. Comparing it to the patterns for bulk Zn foil and ZnO standard, we found that the postreaction sample is neither metallic Zn nor ZnO (Figure 3c). It is likely that an amorphous zinc oxide was formed, considering that no long distance peak was observed in the EXAFS pattern (black curve, Figure 3c).

The dynamic change of Zn oxidation state during CO_2 electrolysis was also probed by in operando XAS techniques. As far as we know, this is the first attempt to utilize this technique in CO_2 electrolysis, which enables us to monitor the structure of Zn catalyst at work. At potentials more negative than −0.7 V, no change of Zn oxidation state occurred in the Zn dendrite catalyst throughout the whole CO_2 electrolysis process, suggesting that Zn catalyst is stable during 1 h electrolysis. An example of this stability is shown in Figure S9. When a less-negative potential was used (e.g. −0.5 V) in operando XANES results (Figure 3d) showed a clear continuous change of Zn oxidation state. In 1 h electrolysis, the Zn dendrite catalyst was fully oxidized to Zn^{2+}, in good agreement with in situ XAS data and SEM results. These observations are also consistent with Zn Pourbaix diagram. It should be noted that in the constant potential electrolysis, an oxidation current was observed for the Zn dendrite electrode in a 2 h experiment (Figure S7), suggesting a severe oxidation reaction occurring at the Zn electrode surface.

CONCLUSION

In summary, a Zn dendrite catalyst was synthesized for high-performance CO_2 conversion to CO in neutral electrolyte at ambient conditions. The Zn dendrite catalyst exhibited remarkable properties in electrochemical CO_2 reduction, an order of magnitude higher activity and around 3-fold higher CO faradaic efficiency than those of bulk Zn counterparts. The discrepancy in CO faradaic efficiencies for bulk Zn electrode in the literature may be resulted from the dissolution of Zn from electrode surface and redeposition under CO_2 electrolysis conditions (i.e., a very negative potential). Detailed structural

DOI: 10.1021/acscatal.5b00922
ACS Catal. 2015, 5, 4586−4591

characterizations including postreaction SEM and in situ/operando XAS measurements explored the stability of Zn electrode at CO_2 electrolysis conditions. We have demonstrated that the Zn catalysts experienced severe chemical oxidation to Zn^{2+} at potentials less negative than −0.7 V, whereas at more negative potentials, they are structurally stable under working conditions. In situ electrodeposition is an effective approach to overcome sensitivity of Zn electrode and to achieve high performance.

■ ASSOCIATED CONTENT

Supporting Information

The Supporting Information is available free of charge on the ACS Publications website at DOI: 10.1021/acscatal.5b00922.

XPS results, formate faradaic efficiency, additional SEM images, hydrogen partial current density data, current profile, fitting of krypton gas adsorption/desorption experiment, and photograph of in situ/operando XAS cell (PDF)

■ AUTHOR INFORMATION

Corresponding Author

*E-mail: jiao@udel.edu.

Notes

The authors declare no competing financial interest.

■ ACKNOWLEDGMENTS

The authors thank the National Science Foundation Faculty Early Career Development program (Award No. CBET-1350911) and the DE NASA EPSCoR/RID program for financial support.

■ REFERENCES

(1) Rosen, B. A.; Salehi-Khojin, A.; Thorson, M. R.; Zhu, W.; Whipple, D. T.; Kenis, P. J. A.; Masel, R. I. *Science* **2011**, *334*, 643−644.

(2) Qiao, J.; Liu, Y.; Hong, F.; Zhang, J. *Chem. Soc. Rev.* **2014**, *43*, 631−675.

(3) Lim, R. J.; Xie, M.; Sk, M. A.; Lee, J. M.; Fisher, A.; Wang, X.; Lim, K. H. *Catal. Today* **2014**, *233*, 169−180.

(4) Kuhl, K. P.; Hatsukade, T.; Cave, E. R.; Abram, D. N.; Kibsgaard, J.; Jaramillo, T. F. *J. Am. Chem. Soc.* **2014**, *136*, 14107−14113.

(5) Hori, Y. In *Modern Aspects of Electrochemistry*; Vayenas, C. G., White, R. E., Gamboa-Aldeco, M. E., Eds.; Springer: New York, **2008**; Vol. *42*, pp 89−189.

(6) Reske, R.; Mistry, H.; Behafarid, F.; Roldan Cuenya, B.; Strasser, P. *J. Am. Chem. Soc.* **2014**, *136*, 6978−6986.

(7) Azuma, M.; Hashimoto, K. *J. Electrochem. Soc.* **1990**, *137*, 1772−1778.

(8) Hori, Y.; Wakebe, H.; Tsukamoto, T.; Koga, O. *Electrochim. Acta* **1994**, *39*, 1833−1839.

(9) Sen, S.; Liu, D.; Palmore, G. T. R. *ACS Catal.* **2014**, *4*, 3091−3095.

(10) Zhang, S.; Kang, P.; Meyer, T. J. *J. Am. Chem. Soc.* **2014**, *136*, 1734−1737.

(11) Tornow, C. E.; Thorson, M. R.; Ma, S.; Gewirth, A. A.; Kenis, P. J. A. *J. Am. Chem. Soc.* **2012**, *134*, 19520−19523.

(12) Kim, D.; Resasco, J.; Yu, Y.; Asiri, A. M.; Yang, P. *Nat. Commun.* **2014**, *5*, 4948.

(13) Li, C. W.; Kanan, M. W. *J. Am. Chem. Soc.* **2012**, *134*, 7231−7234.

(14) Zhu, W.; Michalsky, R.; Metin, Ö.; Lv, H.; Guo, S.; Wright, C. J.; Sun, X.; Peterson, A. A.; Sun, S. *J. Am. Chem. Soc.* **2013**, *135*, 16833−16836.

(15) Manthiram, K.; Beberwyck, B. J.; Alivisatos, A. P. *J. Am. Chem. Soc.* **2014**, *136*, 13319−13325.

(16) Lu, Q.; Rosen, J.; Zhou, Y.; Hutchings, G. S.; Kimmel, Y. C.; Chen, J. G.; Jiao, F. *Nat. Commun.* **2014**, *5*, 3242.

(17) Ikeda, S.; Hattori, A.; Maeda, M.; Ito, K.; Noda, H. *Electrochemistry* **2000**, *68*, 257−261.

(18) Ikeda, S.; Hattori, A.; Ito, K.; Noda, H. *Electrochemistry* **1999**, *67*, 27−33.

(19) Hori, Y.; Kikuchi, K.; Suzuki, S. *Chem. Lett.* **1985**, 1695−1698.

(20) Wang, R. Y.; Kirk, D. W.; Zhang, G. X. *J. Electrochem. Soc.* **2006**, *153*, C357−C364.

(21) Ravel, B.; Newville, M. *J. Synchrotron Radiat.* **2005**, *12*, 537−541.

(22) Desai, D.; Wei, X.; Steingart, D. A.; Banerjee, S. *J. Power Sources* **2014**, *256*, 145−152.

(23) Lee, C. H.; Kanan, M. W. *ACS Catal.* **2015**, *5*, 465−469.

(24) Chen, Y.; Li, C. W.; Kanan, M. W. *J. Am. Chem. Soc.* **2012**, *134*, 19969−19972.

(25) Lu, Q.; Rosen, J.; Jiao, F. *ChemCatChem* **2015**, *7*, 38−47.

DOI: 10.1021/acscatal.5b00922
ACS Catal. 2015, 5, 4586−4591